Hirayama *et al.*
Journal of Electrical Systems and Inf Technol (2024) 11:29
https://doi.org/10.1186/s43067-024-00154-0

Journal of Electrical Systems and Information Technology

RESEARCH Open Access

Design of CRLH-TL BPF with controllable attenuation poles

Atsuya Hirayama[1*], Hinata Ishikawa[1] and Takanobu Ohno[1]

*Correspondence:
hirayama.knct@gmail.com

[1] Advanced Course of Mechanical and Electrical Engineering, National Institute of Technology, Kisarazu College, Chiba, Japan

Abstract

Compact and pole-controllable resonators and bandpass filter (BPF) using a composite right/left-handed transmission line (CRLH-TL) are designed in this study. The distributed constant line in the CRLH-TL has applied a tap-coupling technique, and one tap-coupled stub is loaded with the left-handed (LH) circuit. Attenuation poles are generated when the input susceptance of the stub diverges. In the tap-coupled CRLH-TL resonator, the attenuation pole is controlled at either the desired lower or higher region frequency than a resonant frequency by adjusting the circuit parameters. Also, the BPF constructed by the CRLH-TL resonators is designed based on a filter design theory, where the attenuation poles are located at lower and higher region frequencies than a negative-first-order frequency. The BPF with microstrip structure is fabricated using MEGTRON6 R-5775 (ε_r: 3.7, h: 0.63 mm, t: 18 µm), chip capacitors, and wire inductors. The simulated results show that the desired characteristics are approximately satisfied, i.e., we can design the CRLH-TL BPF which is controllable for the attenuation poles at both lower and higher region frequencies than a resonant frequency. The measured results are good agreement with the simulation. The negative-first-order frequency is generated at 2.00 GHz with 133 MHz bandwidth, i.e., the fractional bandwidth is 6.65 %. The resonator lengths in the BPF are shortened by 81.5 % and 75.0 % in comparison with a conventional half-wavelength ($\lambda/2$) openstub, and the size of the fabricated BPF is 0.18 $\lambda_g \times 0.17\ \lambda_g$. Therefore, a compact BPF with two controllable attenuation poles is realized by the tap-coupled CRLH-TL.

Introduction

Bandpass filters (BPFs) used in RF circuits should be compact and have steep skirt characteristics. Generally, adding the number of filter stages increases the gradient of the transmission characteristics near the passband, which suppresses unwanted signals more. However, the circuit becomes larger due to the increase in the number of circuit elements, which means there is a trade-off between circuit miniaturization and steepness of the skirt characteristics. To solve this problem, some methods generating the attenuation poles near the passband are proposed. For instance, filters using cross-coupling and elliptic function filters are listed [1, 2]. In addition, the research has been reported on BPFs that use a technique called the tap-coupling method, where an input/output section is placed in the middle of the transmission line (TL) [3, 4]. This technique has the unique feature that the attenuation poles can be easily controlled by adjusting

the circuit parameters so that the input susceptance of the tap-coupled stub diverges. However, BPFs using only right-handed (RH) circuits still increase the size inversely proportional to the resonant frequency, and there is a limit to miniaturization even for filters with a small number of stages. Therefore, the research on filters and antennas using composite right/left-handed (CRLH)-TL, which enable circuit miniaturization, has been actively studied in recent years [5–7]. The CRLH-TL BPFs of [8, 9] are realized in sizes 0.51 $\lambda_g \times 0.37\ \lambda_g$ and 0.20 $\lambda_g \times 0.22\ \lambda_g$, which are smaller than conventional BPFs consisting of only RH circuits. By applying the tap-coupling to a CRLH-TL, it is possible to realize compact BPFs with controllable attenuation poles [10]. However, to the best of the authors' knowledge, there have been few studies on the control of attenuation poles in a CRLH-TL BPF applied tap-coupling.

In this study, the resonators in which the distributed constant line is applied a tap-coupling and loaded with the left-handed (LH) circuit are designed. The attenuation pole is located by the tap-coupled stub loaded with the LH circuit at the lower or higher frequency region than negative-first resonance. Next, the BPF composed of the tap-coupled CRLH-TL resonators is designed based on the classical design theory of filters [11]. The parallel resonant circuit in the two-stage BPF including the J-inverter is replaced with a tap-coupled CRLH-TL resonator under a narrow-band approximation [12]. The designed BPF is fabricated, and the S-parameters of the BPF are analyzed and measured by a circuit simulator software and a vector network analyzer (VNA), respectively. This study aims to realize the compact CRLH-TL BPF which can control multiple attenuation poles.

Dispersion diagram of each circuit

Figure 1 shows a tap-coupled resonator loaded with LH circuit, where L_L and C_L are LH inductor and capacitor, l_1 and l_2 are stub length, Z_0 is characteristic impedance, and C_{in} and C_{out} are input/output (I/O) capacitors, respectively. Before designing the resonators, we investigate that the resonator in Fig. 1 is a CRLH-TL by using a dispersion diagram (DD).

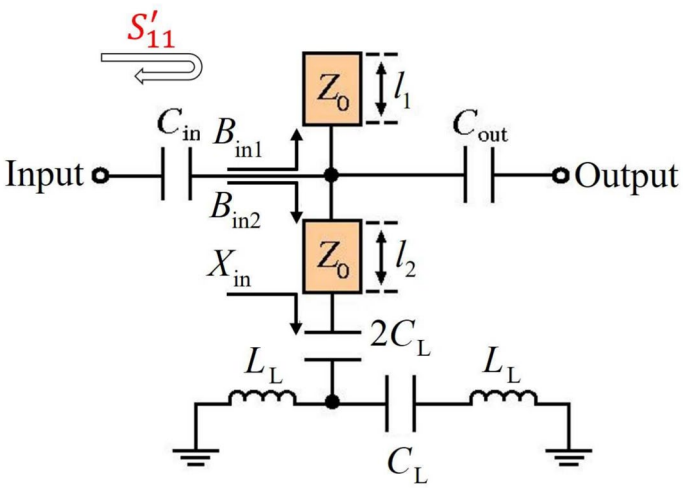

Fig. 1 The schematic of the tap-coupled resonator loaded with LH circuits

When a TL is lossless, the DD is generally defined as

$$\phi = \cos^{-1}\left(\frac{1-\dot{S}_{11}\dot{S}_{22}+\dot{S}_{12}\dot{S}_{21}}{2\dot{S}_{21}}\right) \tag{1}$$

where ϕ and $\dot{S}_{ij}(i,j=1,2)$ are the phase delay and S-parameters in the 2-port circuit [13]. If the 2-port circuit is symmetrical and impedance-matched, $\dot{S}_{12}=\dot{S}_{21}=e^{-j\theta}$ and $\dot{S}_{11}\approx\dot{S}_{22}\approx 0$ and DD is conveniently expressed by

$$\phi \approx \theta \tag{2}$$

instead of Eq. (1), where theta is the phase of $\dot{S}_{21}$. Figure 2a and b shows a distributed constant line (RH-TL) and a 2-cell T-type LH circuit, where l in Fig. 2a is stub length. The DDs θ_{RH} and θ_{LH}, i.e., the phase of $\dot{S}_{21}$ in Fig. 2a and b can be calculated as

$$\theta_{\mathrm{RH}} = \beta l \tag{3}$$

$$\theta_{\mathrm{LH}} = \tan^{-1}\left\{\frac{A(B+R^2C)}{R(A^2-BC)}\right\} \tag{4}$$

$$A = 1-\frac{1}{2\omega^2 C_{\mathrm{L}} L_{\mathrm{L}}} \tag{5}$$

$$B = -\frac{1}{\omega C_{\mathrm{L}}}+\frac{1}{4\omega^3 C_{\mathrm{L}}^2 L_{\mathrm{L}}} \tag{6}$$

$$C = -\frac{1}{\omega L_{\mathrm{L}}}. \tag{7}$$

Note that β is the phase constant, R is the terminal resistance (50 Ω), and ω is the angular frequency. $A(=D), B$, and C in Eqs. (4)–(7) indicate the $ABCD$ parameters of the 1-cell T-type LH circuit. However, the proper DD of the circuit which only consists stubs such as Fig. 1 cannot be derived by Eq. (2) because ϕ is constant. According to reference [14], the DD can be equivalently defined by the phase of the reflection characteristics S'_{11}

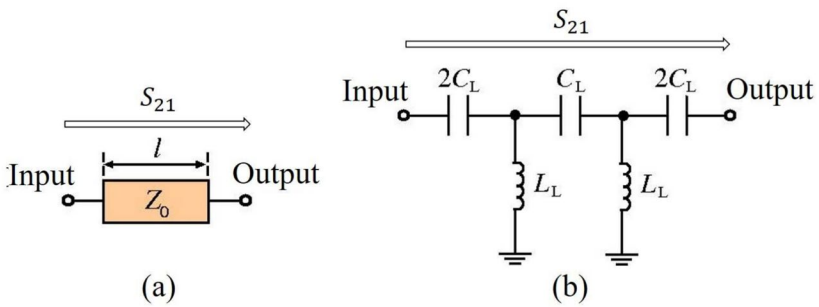

Fig. 2 The schematics of **a** distributed constant line and **b** 2-cell T-type LH circuit. Note that **a** is one of RH-TL

when C_{in} and C_{out} are excluded and Port "Output" is opened to make it a 1-port circuit. S'_{11} is represented as

$$S'_{11} = e^{-j2\theta'} \tag{8}$$

$$\theta' = \tan^{-1}\{(B_{\text{in1}} + B_{\text{in2}})R\} \tag{9}$$

$$B_{\text{in1}} = \frac{\tan \beta l_1}{Z_0} \tag{10}$$

$$B_{\text{in2}} = \frac{1}{Z_0}\frac{X_{\text{in}} \tan \beta l_2 - Z_0}{X_{\text{in}} + Z_0 \tan \beta l_2} \tag{11}$$

$$X_{\text{in}} = \frac{\omega L_{\text{L}}(1 - \omega^2 L_{\text{L}} C_{\text{L}})}{1 - 2\omega^2 L_{\text{L}} C_{\text{L}}} - \frac{1}{2\omega C_{\text{L}}} \tag{12}$$

where B_{in1} is the input susceptance of the openstub, B_{in2} is the input susceptance of the stub loaded with LH circuits, and X_{in} is the input reactance of the LH circuit. From Eqs. (8)–(12), the equivalent DD is the phase of S'_{11} divided by two and depends on the product of the whole input susceptance and the terminal resistance.

Figure 3 shows the DD for each of the three circuits shown in Figs. 1 and 2. Note that the DDs of Figs. 1, 2a, and b are calculated by Eqs. (9), (3), and (4), respectively, where the circuit parameters are written in the title of Fig. 3. It is confirmed that the DD of the RH-TL is always positive in phase and varies linearly from 0 degrees, while the DD of the LH circuit is always negative in phase and varies nonlinearly. Therefore, the DD of

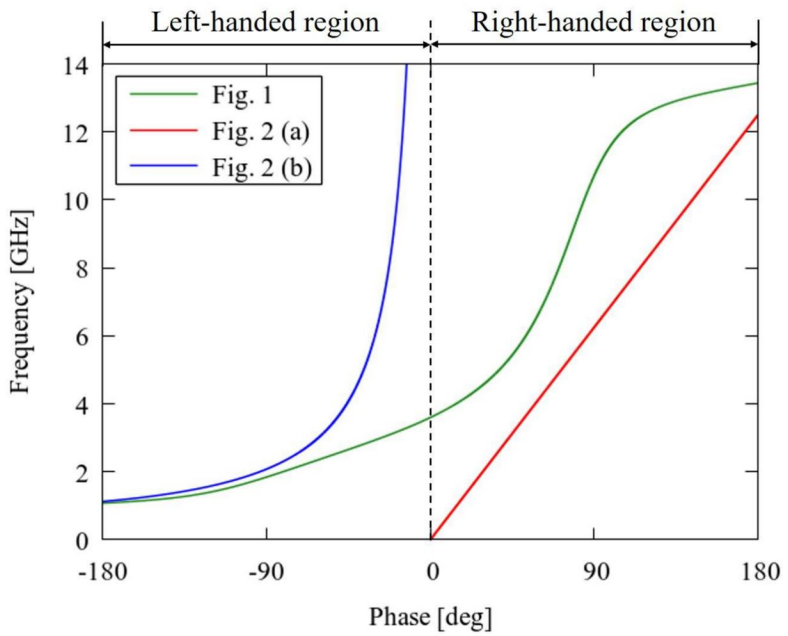

Fig. 3 The DDs of the circuits shown in Figs. 1 and 2 ($l = 12$ [mm], $Z_0 = 50$ [Ω], $C_{\text{L}} = 2$ [pF], $L_{\text{L}} = 5$ [nH], $l_1 = 7$ [mm], and $l_2 = 5$ [mm])

the CRLH-TL has the respective characteristics of the RH-TL and the LH circuit, and the phase changes from the negative region to the positive region. Focusing on the DD in Fig. 1, we can see from Fig. 3 that the phase is in the negative region at 0–3.597 GHz and in the positive region from 3.597 GHz and beyond. Therefore, from Fig. 3, it can be verified that the tap-coupled resonator loaded with LH circuit in Fig. 1 is a CRLH-TL. However, the resonator in Fig. 1 is regarded as RH-TL when C_{L} equals 0 pF because the resonator is constructed by only openstubs.

Tap-coupled resonators loaded with LH circuit

Next, the tap-coupled CRLH-TL resonators in Fig. 1 are designed. Note that C_{in}, C_{out} are inserted into the I/O section to facilitate confirming resonance by under-coupling. In this study, the resonators are designed according to the specifications shown in Table 1, where f_{-1} is a negative-first-order frequency and f_{att} is an attenuation pole. As for the control of f_{att}, it is located at the distributed constant line loaded with the LH circuit in Fig. 1. The advantage of controlling f_{att} in the stub is that there is the possibility to shorten the stub length when f_{att} is a low frequency. If f_{att} is controlled by the open-stub, the stub length increases as f_{att} decreases. On the other hand, depending on the values of such as L_{L} and C_{L}, the stub length may be shorter than in the case of an open-stub. Therefore, f_{att} is located using the stub loaded with the LH circuit in this study. The circuit parameters for each type of resonator can be obtained from Eqs. (10)–(12) expressed by

$$B_{\mathrm{in1}} + B_{\mathrm{in2}} = 0 \ \ (\mathrm{at}\, f = f_{-1}), \tag{13}$$

$$B_{\mathrm{in2}} = \infty \ \ (\mathrm{at}\, f = f_{\mathrm{att}}). \tag{14}$$

If Eq. (13) (the resonance condition) and Eq. (14) (the condition of realizing an attenuation pole) are satisfied simultaneously, Z_0, l_1, l_2, C_{L}, and L_{L} are determined in Table 2. Also, C_{in} and C_{out} of Type 1-6 resonators are 0.10 pF to make f_{-1} sharp. We simulate the transmission characteristic $|\dot{S}_{21}|$ and B_{in2} of the resonators using a circuit simulator.

Figures 4, 5, 6, 7 are the simulated $|\dot{S}_{21}|$ and B_{in2} of the resonator of Type 1-6. Figures 4 and 6 show that each f_{-1} is generated during 1.96−1.98 GHz and each f_{att} is confirmed at desired frequency. The error in f_{-1} should be caused due to C_{in} and C_{out} which are not taken into account when designing the resonators. Moreover, each B_{in2} in Figs. 5 and 7 diverges at each f_{att} in Figs. 4 and 6, which means f_{att} can be controlled by the

Table 1 The design specifications of the resonators

Type	f_{-1} [GHz]	f_{att} [GHz]
1	2.00	1.40
2		1.55
3		1.70
4		2.70
5		2.85
6		3.00

Table 2 The obtained circuit parameters of the CRLH-TL resonators

Type	C_L [pF]	L_L [nH]	Z_0 [Ω]	l_1 [mm]	l_2 [mm]
1	1.18	2.36	75.00	6.21	8.69
2	0.95	2.84	59.00	6.93	6.12
3	0.55	4.37	44.25	7.31	6.29
4	1.22	2.11	51.25	6.27	12.42
5	1.59	1.66	38.25	6.57	9.43
6	1.05	2.59	61.25	7.18	6.61

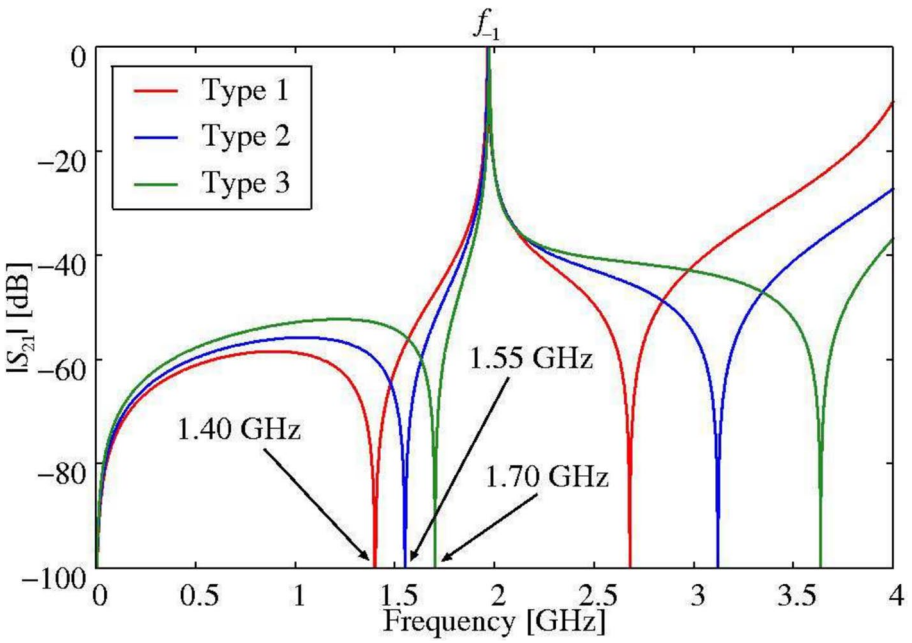

Fig. 4 The simulated $|\dot{S}_{21}|$ of each designed resonator (Type 1-3)

tap-coupled distributed constant line loaded with LH circuit. Thus, the tap-coupled CRLH-TL resonators are capable of controlling f_{att} at either lower or higher region frequencies than f_{-1}.

Design and fabrication of tap-coupled CRLH-TL BPF

Figure 8 and Table 3 show the CRLH-TL BPF using the tap-coupled resonators shown in Fig. 1 and the specifications of the BPF, respectively. Note that N, C_{r1} and C_{r2}, f_{-1}, Δf, and f_{attx} (x=1, 2) are the number of stages, the capacitances of the parallel resonators, the negative-first-order frequency, the bandwidth, and the attenuation poles, respectively. We design the CRLH-TL BPF in accordance with the steps as follows;

1. The lumped-element BPF including J-inverters is designed based on a classical design method [11].
2. The parallel resonators in the lumped-element BPF are replaced with the tap-coupled CRLH-TL resonators using a narrow-band approximation [12].

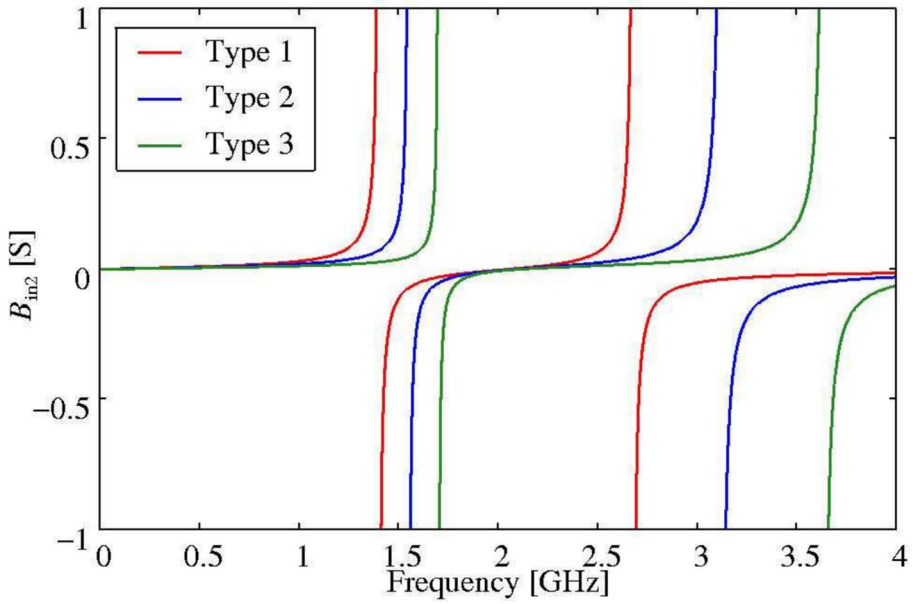

Fig. 5 The simulated B_{in2} of each designed resonator (Type 1-3)

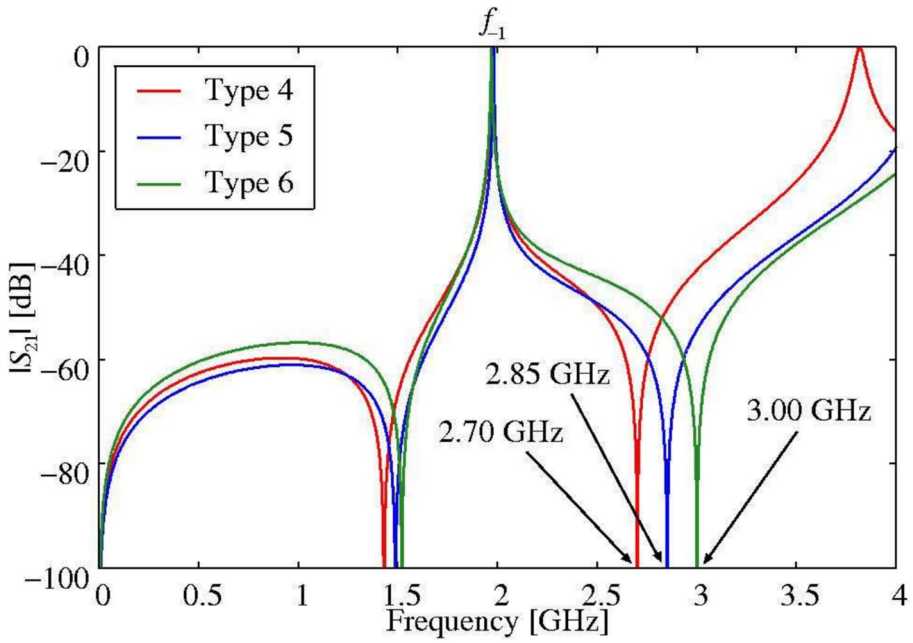

Fig. 6 The simulated $|\dot{S}_{21}|$ of each designed resonator (Type 4-6)

3. The circuit parameters of the CRLH-TL BPF shown in Fig. 8 are calculated.

Figure 9 shows a lumped-element BPF including J-inverters. Firstly, the BPF in Fig. 9 meeting with the specifications shown in Table 3 is designed. The circuit parameters such as C_{in} and C_{out} and the gap capacitor C_g are obtained according to [11]. Secondly, the parallel

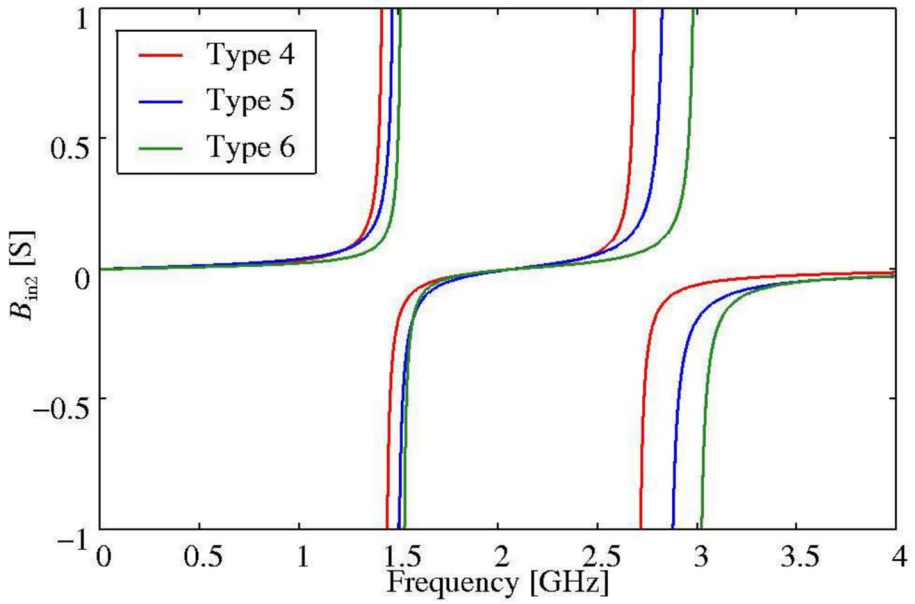

Fig. 7 The simulated B_{in2} of each designed resonator (Type 4-6)

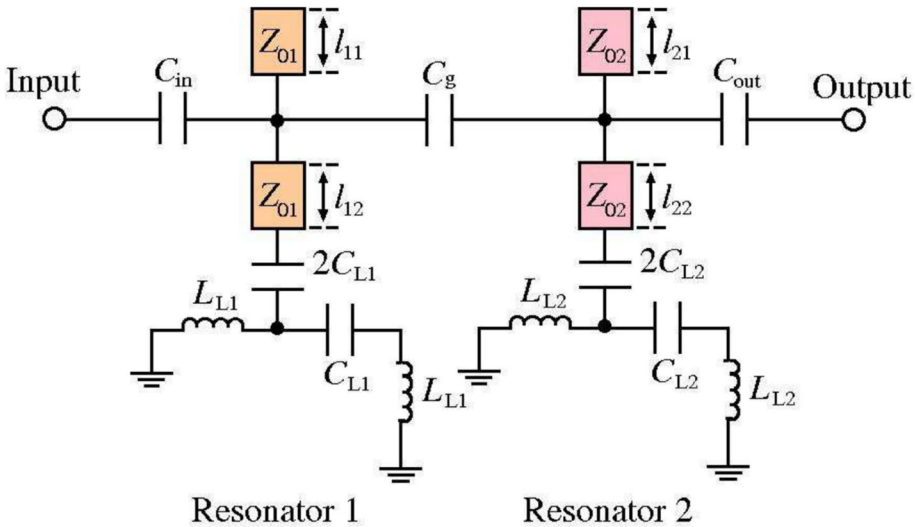

Fig. 8 The circuit schematic of the tap-coupled CRLH-TL BPF

Table 3 The design specifications of the tap-coupled CRLH-TL BPF

Filter response	N [−]	C_{r1}, C_{r2} [pF]	f_{-1} [GHz]	Δf [MHz]	f_{att1} [GHz]	f_{att2} [GHz]
Butterworth	2	8.00	2.00	150	1.55	2.70

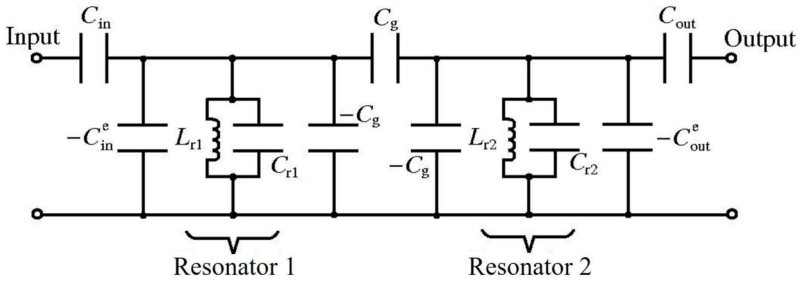

Fig. 9 The BPF schematic including J-inverter

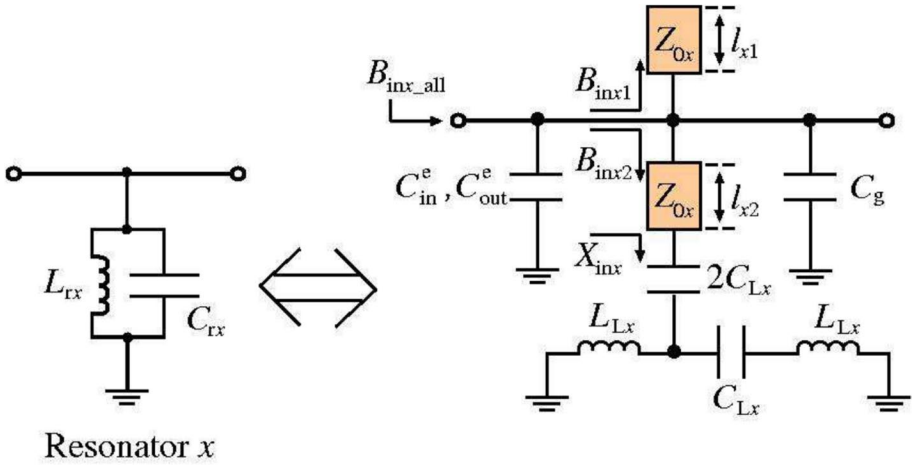

Fig. 10 Replacement of the parallel resonant circuits to the CRLH-TL resonators

resonators are replaced with the tap-coupled CRLH-TL resonators shown in Fig. 10. We note that the capacitance C^e_{in}, C^e_{out}, and C_g in Fig. 10 are connected in parallel due to canceling the negative elements in Fig. 9. The replacement of the resonators is executed based on a narrow-band approximation [12], where the following equations

$$B_{inx\_all} = B_{inx1} + B_{inx2} + \omega(C_g + C^e_{in}) = 0 \ \ (\text{at} f = f_{-1}), \tag{15}$$

$$B_{inx1} = \frac{\tan \beta l_{x1}}{Z_{0x}}, \tag{16}$$

$$B_{inx2} = \frac{1}{Z_{0x}} \frac{X_{inx} \tan \beta l_{x2} - Z_{0x}}{X_{inx} + Z_{0x} \tan \beta l_{x2}} = \infty \ \ (\text{at} f = f_{attx}), \tag{17}$$

$$X_{inx} = -\frac{1}{2\omega C_{Lx}} + \frac{\omega L_{Lx}(1 - \omega^2 L_{Lx} C_{Lx})}{1 - 2\omega^2 L_{Lx} C_{Lx}}, \tag{18}$$

$$b_x = b_{xb} - b_{xa} = \frac{\omega}{2} \frac{\mathrm{d}B_{inx\_all}}{\mathrm{d}\omega} - \omega C_{rx} = 0 \ \ (\text{at} f = f_{-1}) \tag{19}$$

are used. Note that $B_{\mathrm{in}x\_\mathrm{all}}$ is the input susceptance of the CRLH-TL resonator, $B_{\mathrm{in}x1}$ and $B_{\mathrm{in}x2}$ are the input susceptances of the openstub and the distributed constant line loaded with LH circuit, respectively.

Also, $X_{\mathrm{in}x}$ is the input reactance of the LH circuit and b_x is the relational expression between the susceptance slope parameters of the parallel resonators and the tap-coupled CRLH-TL resonators. The attenuation poles are located by the distributed constant line loaded with LH circuit as well as the design of the CRLH-TL resonators. The conditions that Eqs. (15), (17), and (19) (the condition of realizing a bandwidth) should be satisfied when replacing the resonators as in Fig. 10. Finally, the circuit parameters such as the characteristic impedance Z_{0x}, the stub length l_{x1} and l_{x2}, and LH inductance/capacitance $L_{\mathrm{L}x}$ and $C_{\mathrm{L}x}$ are obtained. The flow of replacing the resonators and calculating each circuit parameter is performed according to the flowchart shown in Fig. 11. Calculating Z_{0x}, l_{x2}, $L_{\mathrm{L}x}$, $C_{\mathrm{L}x}$, and l_{x1} simultaneously would take a great deal of time. However, Fig. 11 shows that Z_{0x}, l_{x2}, $L_{\mathrm{L}x}$, and $C_{\mathrm{L}x}$ can be calculated prior to l_{x1}. This is because l_{x1} is independent of the condition of Eq. (17) so that it takes less time

than the method of calculating five circuit parameters at the same time. After obtaining four circuit parameters, l_{x1} is calculated by Eqs. (15) and (19), and each circuit parameter is shown in Table 4. Figure 12 shows the S-parameters simulated by a circuit simulator. The simulated results show that f_{-1}, $f_{\mathrm{att}1}$, and $f_{\mathrm{att}2}$ are generated at 2.00 GHz, 1.55 GHz, and 2.70 GHz, respectively. Also, Δf is 154 MHz which means the error rate of Δf is 2.67 %. The error in Δf should be caused when replacing the resonators under the condition of a narrow-band approximation, which is inevitable. However, the characteristics of the CRLH-TL BPF are approximately satisfied and the attenuation poles are confirmed at the desired low/high region frequency than f_{-1}. In addition, the total length of Resonators 1 and 2 in Fig. 8 is 13.85 mm and 18.75 mm. The length of a conventional half-wavelength ($\lambda/2$) resonator is 74.95 mm when the resonant frequency is 2.00 GHz, i.e., Resonators 1 and Resonator 2 are 81.5 % and 75.0 % shorter than $\lambda/2$ resonator. The significant miniaturization of the resonator length should be the effect on the LH circuit. Therefore, we can design the compact CRLH-TL BPF with two controllable attenuation poles.

Next, we fabricate the BPF using a substrate with MEGTRON6 R-5775 (dielectric constant ε_{r}: 3.7, substrate thickness h: 0.63 mm, and metal thickness t: 18 μm) and Mits Electronics Seven Mini based on the parameters shown in Table 4. Figure 13a and b shows the structure and top view of the BPF with a flat ground plane, where the CRLH-TL resonators are bent to suppress the stray coupling between the resonators. Note that $l_{\mathrm{p}1}$, $l_{\mathrm{p}2}$, l_{f}, $w_{\mathrm{w}1}$, w_2, w_{f}, s, and s_{t} in Fig. 13a indicate the pad length, the feed line length, the width of Resonator 1 and Resonator 2, the feed line width, the gap to place capacitors, and the gap to ground inductors, respectively. In this study, the inductors and the capacitors are realized by chip capacitors and a wire inductor (0.20 mm dia.) adjusted the length.

The reason for using the chip elements is to easily confirm the usefulness of the design. Also, the stub lengths written in Fig. 13 are varied from the values of Table 4 due to a wavelength-shortening effect. The pads present at the tip of the resonator are for soldering $C_{\mathrm{L}x}$ and $L_{\mathrm{L}x}$. The thru holes are drilled to make $L_{\mathrm{L}x}$ conductive to the ground. C_{in} and C_{out} are mounted between the input/output and Resonator x, and C_{g} is mounted

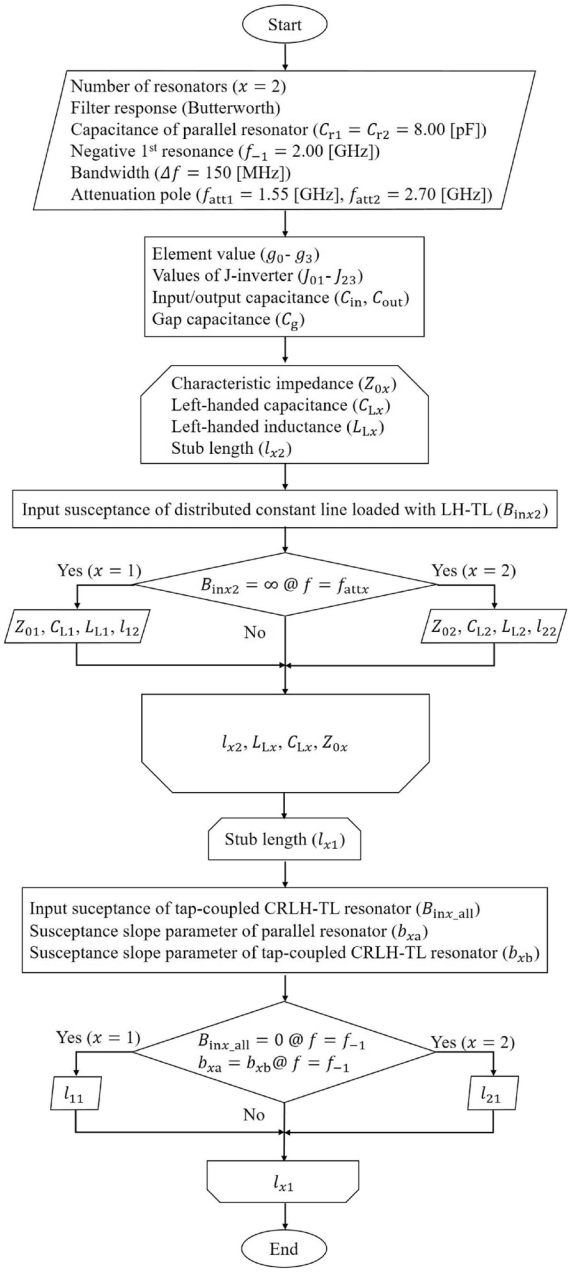

Fig. 11 The flowchart of designing the tap-coupled CRLH-TL BPF

Table 4 The circuit parameters of the BPF

C_g [pF]	C_{in}, C_{out} [pF]	C_{L1} [pF]	L_{L1} [nH]	C_{L2} [pF]	L_{L2} [nH]
0.42	0.96	1.26	1.87	1.68	1.34
Z_{01} [Ω]	**Z_{02} [Ω]**	**l_{11} [mm]**	**l_{12} [mm]**	**l_{21} [mm]**	**l_{22} [mm]**
59.00	51.88	6.10	7.75	6.20	12.55

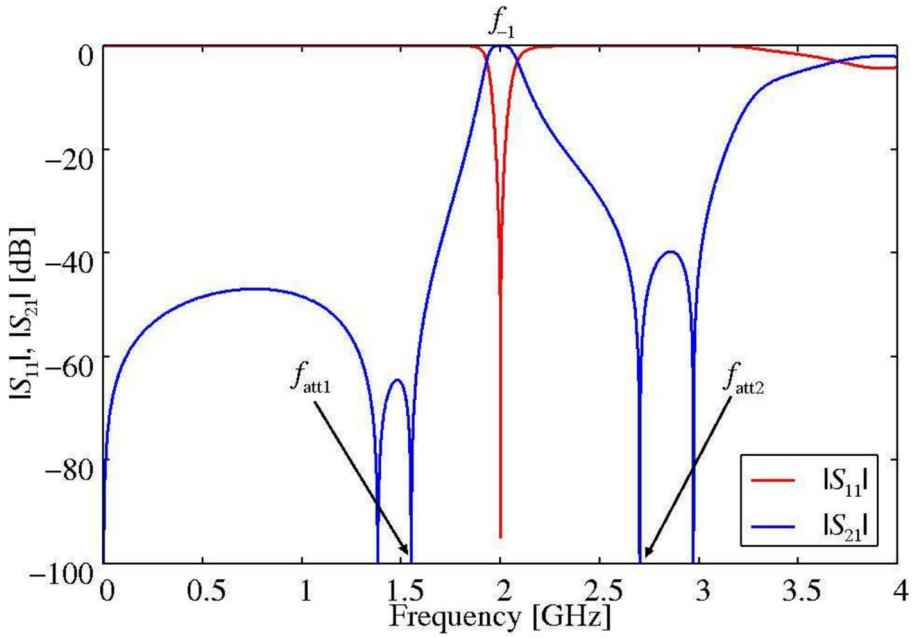

Fig. 12 The simulated S-parameters of the CRLH-TL BPF

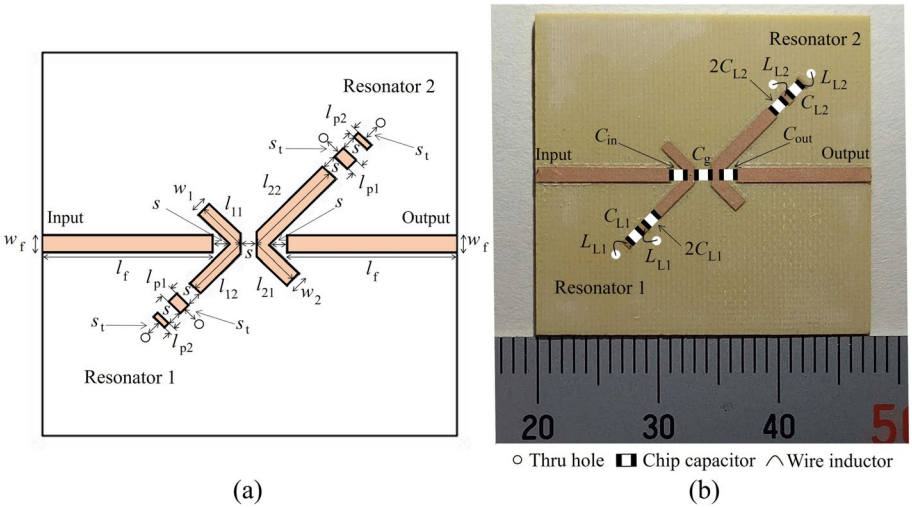

Fig. 13 **a** The structure of the CRLH-TL BPF. **b** The fabricated CRLH-TL BPF. Their corresponding parameters are as follows: l_{11}=3.63 [mm], l_{12}=4.62 [mm], l_{21}=3.66 [mm], l_{22}=7.41 [mm], l_{p1}=0.80 [mm], l_{p2}=0.40 [mm], l_f =12.27 [mm], w_1=1.04 [mm], w_2=1.30 [mm], w_f=1.38 [mm], s=1.20 [mm], and s_t=1.00 [mm]

between Resonator 1 and Resonator 2, respectively. After soldering these components on the substrate, the S-parameters of the BPF are measured using Agilent (now Keysight Technologies) E5071C-2D5 ENA Series Network Analyzer shown in Fig. 14 and compared with the simulated results. A short-open-load-thru calibration is mechanically conducted to remove the effect of the measurement equipment and cables by using Keysight Technologies 85052D 3.5mm economy calibration kit. The range of frequency is between 300 kHz and 6 GHz, and the number of plots is 1601. Also, the IF bandwidth and the input power of VNA are 70 kHz and -5 dBm in this study.

Fig. 14 The measurement setup of the fabricated CRLH-TL BPF

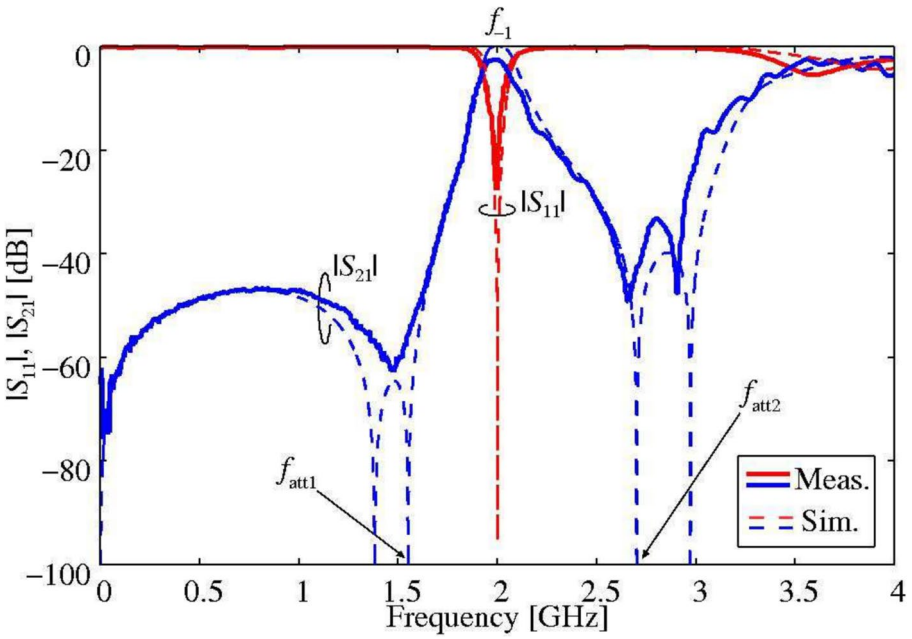

Fig. 15 The measured S-parameters of the CRLH-TL BPF with the simulated results

The S-parameters of the CRLH-TL BPF are shown in Fig. 15, where the dotted lines are the simulated results and the solid lines are the measured results, respectively. From the measured results, the attenuation poles of the lower region unite and it is confirmed that f_{-1}, Δf, and f_{att2} are 2.00 GHz, 130 MHz, and 2.66 GHz, which mean Δf is 15.6 % narrower than simulated results and f_{att2} is slightly shifted toward

the lower region. The major reason for the errors in the transmission characteristics should be caused by the tolerance of the chip capacitors and the wire inductors, stray capacitors, and edge effects. Also, the insertion loss and return loss at f_{-1} are 2.47 dB and 30.9 dB, respectively. It is believed that the resistance components of the chip elements should make the S-parameters worse and the improvement is prospected by using quasi-lumped elements such as interdigital capacitors and spiral inductors with less loss instead of chip elements [15]. However, most parts of the S-parameters are good agreement with the theoretical and measured results. Moreover, the size of the CRLH-TL BPF is 16.21 mm × 15.01 mm or 0.18 λ_g× 0.17 λ_g, where $\lambda_g = 88.38$ mm corresponds to the guided wavelength using MEGTRON6 at the frequency of 2.00 GHz. The performance comparison with previously published BPFs is listed in Table 5. From Table 5, it is confirmed that the size of the fabricated filter is smaller than that of the present filters. The BPF in this study is similar to [16, 17] in having attenuation poles; however, notably, this work can freely control attenuation poles both near and far from the passband.

Therefore, a compact BPF with two controllable attenuation poles is realized by using the tap-coupled CRLH-TL resonators.

Conclusion

Resonators and BPFs using tap-coupled CRLH-TL were studied in this work. In the CRLH-TL resonators, an attenuation pole can be controlled to the desired frequency in either the lower or higher region than a negative-first-order frequency. We designed, simulated, and fabricated a prototype BPF composed of the CRLH-TL resonators. The simulation results show that the attenuation poles can be controlled at the designated low and high frequency regions. The S-parameters measured by the VNA agreed well with that of the simulation software analysis. Also, the insertion loss and the return loss at the negative-first-order frequency were 2.47 dB and 30.9 dB, which would be improved by replacing chip capacitors and wire inductors to low loss quasi-lumped elements. Moreover, the total lengths of the CRLH-TL resonators in the BPF were significantly shortened by 81.5 % and 75.0 % compared with a conventional $\lambda/2$ openstub resonator and the size of the fabricated BPF is 0.18 λ_g× 0.17 λ_g. Therefore, a compact and highly selective resonator and BPF were realized by the tap-coupled CRLH-TL. This study contributes to realizing a compact filter with

Table 5 The comparison between the present work

References	CF	FBW	IL	Attenuation pole		Electrical size
	[GHz]	[%]	[dB]	Close to PB	Far from PB	[λ_g × λ_g]
[16]	3.60	6.0	0.98	Yes	Yes	0.44×0.44
[17]	2.40	12.5	0.7	Yes	–	0.31×0.27
[18]	2.40	–	2.5	–	–	0.47×0.14
[19]	2.25	9.4	0.8	–	–	0.24×0.19
This work	2.00	6.65	2.5	Yes	Yes	0.18×0.17

Note that CF, FBW, IL, and PB mean center frequency, fractional bandwidth, insertion loss, and passband, respectively

good characteristics in which attenuation poles can be freely controlled by a simple method, and the CRLH-TL BPF is a promising candidate for the applications of 5G technology such as satellites and mobile communications.

Abbreviations

$\lambda/2$	Half-wavelength
BPF	Bandpass filter
CF	Center frequency
CRLH-TL	Composite right/left-handed transmission line
DD	Dispersion diagram
FBW	Fractional bandwidth
I/O	Input/output
IL	Insertion loss
LH	Left-handed
PB	Passband
RH	Right-handed
VNA	Vector network analyzer

Acknowledgements
Not applicable.

Author contributions
Atsuya Hirayama (A.H.) is the corresponding author, who was involved in the design of the CRLHTL resonators and BPF, simulation setup, and prototype experiment. Hinata Ishikawa (H.I.) simulated the resonators and the BPF. Also, H.I. assisted A.H. in fabricating and measuring the BPF. Takanobu Ohno (T.O.) encouraged A.H. to study the resonators and BPF, verified the design method, and supervised the findings of this work. All authors discussed the results and A.H. wrote the final manuscript with support from H.I. and T.O. All authors read and approved the final manuscript.

Funding
This research received no external funding.

Availability of data and materials
All data generated or analyzed during this study are included in this published article.

Declarations

Competing interests
The authors declare that they have no conflict of interest.

Received: 27 March 2024 Accepted: 14 July 2024
Published online: 22 July 2024

References

1. Ma Z, Kobayashi Y (2001) Theory for the design of a filter having one cross coupling path to realize poles of attenuation in its stopband. Paper presented at APMC 2001, National Taiwan University, Taipei, Taiwan, 3–6 Dec 2001
2. Ishizaki T, Ogawa K, Miyake H (1998) Practical design procedure of an elliptic function dual-mode cavity filter coupled through a non-zero-thick septum. IEICE Trans Electron 81(6):916–923
3. Wada K et al (2002) New tap–coupling technique for improving skirt characteristics of a $\lambda/4$ resonator bandpass filter by placement of attenuation poles. Paper presented at IEEE APCCAS 2002, Denpasar, Indonesia, 28–31 Oct 2002
4. Okuzaki N et al (2010) Dual-band microstrip-line BPFs using tap-coupling resonators. Electron Commun Jpn 93(6):25–33
5. Tian H, Liu H, Song Z (2023) Miniaturized highly selective balanced ultrawideband HTS bandpass filter using CRLH transmission line aided by gray wolf algorithm. IEEE MWTL 33(12):1607–1610
6. Vallappil AK et al (2020) Compact metamaterial based 4×4 butler matrix with improved bandwidth for 5G applications. IEEE Access 8:13573–13583
7. Kushiyama Y, Arima T, Uno T (2018) Study on CRLH leaky–wave antenna using varactor–loaded transmission line resonator. Paper presented at ISAP 2018, Busan, South Korea, 23–26 Oct 2018
8. Hu S et al (2020) Design of a compact 5.7–5.9 GHz filter based on CRLH resonator units. Prog Electromagn Res Lett 89:141–149
9. Wang P et al (2021) A novel miniaturized l-band filter with great stopband characteristics using interdigitated coupled lines CRLH-TL structure. Prog Electromagn Res C 114:57–67
10. Sasanami Y et al (2011) Resonance characteristics of CRLH microstrip line resonators with attenuation poles and their application to bandpass filters. IEICE Tech Rep 111(250):69–74
11. Matthaei GL, Young L, Jones EMT (eds) (1980) Microwave filters, impedance matching networks and coupling structures. Artech House, Boston

12. Ohno T, Wada K, Hashimoto O (2005) Design methodologies of planar duplexers and triplexers by manipulating attenuation poles. IEEE Trans Microw Theory Tech 53(6):2088–2095
13. Caloz C, Itoh T (eds) (2006) Electromagnetic metamaterials: transmission line theory and microwave applications. Wiley, Hoboken, NJ
14. Tanaka S, Mukaida K, Takata K (2015) Compact stub resonators with enhanced q-factor using negative order resonance modes of non-uniform CRLH transmission lines. IEICE Trans Electron 98(3):252–259
15. Hong J-S, Lancaster MJ (eds) (2001) Microstrip filters for RF/microwave applications. Wiley, Hoboken, NJ
16. Sathishkannan P et al (2020) A quasi-elliptic Band Pass Filter designed using quadruplet metamaterial resonators for operation in the 3 GHz (5G) band. Paper presented at APSYM 2020, Cochin, India, 14–16 Dec 2020
17. Ibrahim AA, Abdalla MA, Abdel-Rahman A (2018) Wireless bandpass filters build on metamaterials. Microw RF 57(5):1–8
18. Syahral M, Munir A (2016) Development of multiple elements of SRR-based Bandpass filter. Paper presented at TSSA 2016, Denpasar, Indonesia, 06–07 Oct 2016
19. Choudhary DK et al (2017) A via-less compact bandpass filter with improved selectivity using metamaterial structure. Paper presented at APMC 2017, Kuala Lumpur, South Malaysia, 13–16 Nov 2017

Publisher's Note